Available online at www.sciencedirect.com
SCIENCE DIRECT
Polymer 46 (2005) 4077–4087
polymer
www.elsevier.com/locate/polymer

Atomic force microscopy study of the lamellar growth of isotactic polypropylene

Jian-Jun Zhou[a,1], Ji-Guang Liu[a], Shou-Ke Yan[a], Jin-Yong Dong[a], Lin Li[a,*], Chi-Ming Chan[b,*], Jerold M. Schultz[c,*]

[a]*State Key Laboratory of Polymer Physics and Joint Laboratory of Polymer Science and Materials, Institute of Chemistry, Chinese Academy of Sciences, Beijing 100080, China*
[b]*Department of Chemical Engineering, Hong Kong University of Science and Technology, Clear Water Bay, Hong Kong, China*
[c]*Department of Chemical Engineering, University of Delaware, Newark, DE 19716, USA*

Received 14 September 2004; received in revised form 2 March 2005; accepted 6 March 2005
Available online 18 April 2005

Abstract

The growth behaviors of cross-hatched and lath-like lamellae of α-form spherulites and flat-on lamellae of β-form pherulites of isotactic polypropylene were studied with a high-temperature atomic force microscopy in situ and in real time. The growth rates of crystal lamellae in types I, II and mixed α-form spherulites and in β-form spherulites, as well as the spatial frequency of tangential branching, were measured. The frequency of tangential branching increases with decreasing crystallization temperature, while the growth rates of leading radial and tangential lamellae are approximately the same at a given temperature. Observations of as-crystallized materials demonstrated that the spacing and length of transverse lamellae is sufficient to differentiate among spherulite types. Height measurements in the melt near the growth surface indicate roles of molecular transport in the crystallization process.

Keywords: Crystallization; Lamellar growth; Atomic force microscopy

1. Introduction

When crystallized from its melt, isotactic polypropylene (*i*-PP) can develop different forms of crystals, such as the α-, β-, γ- and mesomorphic forms [1–6]. Using polarizing optical microscopy (POM), Padden and Keith [1] discriminated and classified the polymorphism of *i*-PP spherulites into four types according to the changes in birefringence. Types I, II, and mixed spherulites have a monoclinic lattice referred to as the α-form, with unique cross-hatched lamellar structures, while types III and IV have a trigonal lattice referred to as the β-form. Types I and II exhibit an obvious Maltese cross and can be easily discerned on the basis of their birefringence, which is positive for type I and negative for type II. Types III and IV are highly negatively birefringent and distinct banded spherulites are found in type IV. The mixed α-form spherulites show a coarse mixed birefringent property. Using transmission electron microscopy (TEM), Norton and Keller [7] found that the constituent lamellar-level structures correlate to the polymorphism of *i*-PP. The change in birefringence of types I and II and the mixed α-form spherulites are attributed to the relative amount of tangential lamellae of the crosshatched structures. It is known that the formation of the unique cross-hatched lamellae of α-form *i*-PP spherulites is the result of homoepitaxial growth of lamellar branches and that the tangential lamellae grow epitaxially on the (010) plane of a parent lamella [8–10]. The tangential lamellar branching is favored when isochiral helices of the new crystals set themselves at approximately 80° to the helices on the (010) plane of the parent crystal. Works by Lotz and coworkers suggests that at this setting the near identity of the *a* and *c* axes of the unit cell provides good interdigitation of the methyl groups of parent and daughter crystal [11,12].

When crystallized from the melt, β-form *i*-PP spherulites can also be obtained by various methods, such as

* Corresponding authors. Tel./fax: +86 108 261 9830.
E-mail addresses: lilin@iccas.ac.cn (L. Li), schultz@che.udel.edu (J. M. Schultz).
[1] Present address: Graduate School of the Chinese Academy of Sciences.

0032-3861/$ - see front matter © 2005 Elsevier Ltd. All rights reserved.
doi:10.1016/j.polymer.2005.03.047

crystallizing in a temperature gradient [13–15] or from an oriented melt [16,17], or by adding a selective β-nucleating agent [18–22]. Different from the α-form *i*-PP spherulites, a β-form spherulite usually displays a strong negative birefringence [1,7,21]. It has been observed that β-form *i*-PP lamellar crystals exhibit neither the peculiar lath-like form nor the cross-hatched lamellar morphology of α-form *i*-PP crystals. β-form *i*-PP lamellar crystals are consistently observed to show an extended sheet morphology characterized by frequent giant screw dislocations [7,9,23].

The morphology of *i*-PP crystallized from the melt has been studied extensively over the past few decades using POM [1,7,15,18–21], TEM [7–10,24], scanning electron microscopy [25,26] and atomic force microscopy (AFM) [23,27,28]. Recently, AFM has been recognized as a useful tool for the characterization of lamellar growth of semicrystalline polymers in situ and in real time. Equipped with a hot-stage, tapping-mode AFM with height and phase imaging has been used to observe the lamellar growth behavior of many semi-crystalline polymers, such as polyethylene oxide [29,30], poly(ethylene terephthalate) [31], and polyethylene [32–34], etc. Most recently, Schönherr and coworkers [35,36] studied the morphology and crystallization behavior of a low-crystallinity PP using AFM with a hot stage. The elastomeric PP crystallized to form α-form spherulites, and the cross-hatched lamellae were clearly identified. The early stages of the crystallization and the development of cross-hatching lamellar structures were also observed and their results demonstrated how daughter lamellae grow epitaxially from the mother lamellae.

The present work presents a rather comprehensive AFM study of the crystallization of *i*-PP from the melt. Examination of the polymer crystallized at various temperatures provides an AFM morphological atlas. The lamellar growth behaviors of α- and β-form *i*-PP spherulites were observed in situ and in real time using AFM at elevated temperatures. While some of the work, which covers morphological information is already available in the literature, it is reported here in greater detail. More importantly, the missing detail for the crystallization of the α-form is presented, as well as new information concerning the β-form. Finally, AFM height images reveal effects of slow molecular transport to and from the growth front.

2. Experimental

2.1. Materials and sample preparation

The isotactic polypropylene (*i*-PP) with $\bar{M}_w = 41.2 \times 10^4$ and $\bar{M}_w/\bar{M}_n = 5.5$, as measured by gel permeation chromatography (GPC), was bought from Aldrich. Thin films with a thickness around 200 nm for AFM observations were prepared by spin coating polymer solutions onto a freshly cleaved surface of mica. The *i*-PP was dissolved in boiling *p*-xylene (138 °C) with a concentration of 10 mg ml^{-1}. In order to obtain a smooth surface for the *i*-PP thin films, the mica substrate was heated to 80 °C during spin coating to evaporate the solvent quickly. The films were dried in a vacuum oven at 50 °C for 24 h to remove the solvent. Films with a thickness of 10 μm were prepared by solution casting for optical microscopy observations. The thickness of the *i*-PP films was estimated by AFM. To avoid oxidation, the melting and isothermally crystallization of the *i*-PP films were carried out in Perkin–Elmer DSC cells under N_2 protection. The *i*-PP films were melted at 200 °C for 5 min, and then quickly quenched to a selected temperature to allow an isothermal crystallization for various times.

After crystallization, the thick films (~10 μm) were observed using a POM (Olympus BH-2) fitted with a color sensitive plate to determine the sign of the birefringence. A Panasonic 230 CCD was used to capture the optical microscopy images.

AFM tapping-mode images were acquired using an AFM (NanoScope IIIA Digital Instrument) equipped with a high temperature heater accessory. MultiMode™ Instruments). The measured temperature of the AFM hot-stage was calibrated using a thermocouple held to the mica surface by a magnetic sheet. It has been shown that the measured surface temperature of a thin film of poly(ethylene oxide) with a thickness of 130 nm was overestimated by 0.1 °C at surface temperature of 57 °C [37]. In the current study, the relative temperatures for polymer films with a thickness of about 200 nm should be comparable. The experimental details of high temperature AFM can be found elsewhere [29,31,34]. Topographic and phase images were recorded simultaneously. The setpoint amplitude ratio ($r_{sp} = A_{sp}/A_0$, where A_{sp} is the set-point amplitude and A_0 is the amplitude of the free oscillation) was adjusted to 0.7–0.9. Si tips (TESP, Digital Instruments) with a resonance frequency of approximately 300 kHz and a spring constant of about 40 N m^{-1} were used. The *i*-PP thin films were melted on the AFM hot stage at 200 °C for 4 min, and then isothermally crystallized at a specific temperature under N_2 protection. For the growth of β-lamellae, a selective β-nucleating agent was used to induce the growth of β-form spherulites.

3. Results

3.1. Basic morphological descriptions: spherulites and lamellar structures

Type I α-form *i*-PP spherulites with a clear Maltese cross were obtained when isothermally crystallized at 130 °C, as shown in Fig. 1(a). Positive birefringence was observed using a color sensitive plate. The surface morphology of a spherulite was investigated using AFM, as shown in Fig. 1(b). A fully developed spherulite can be clearly discerned. The unique mesh-type cross-hatched morphology of α form

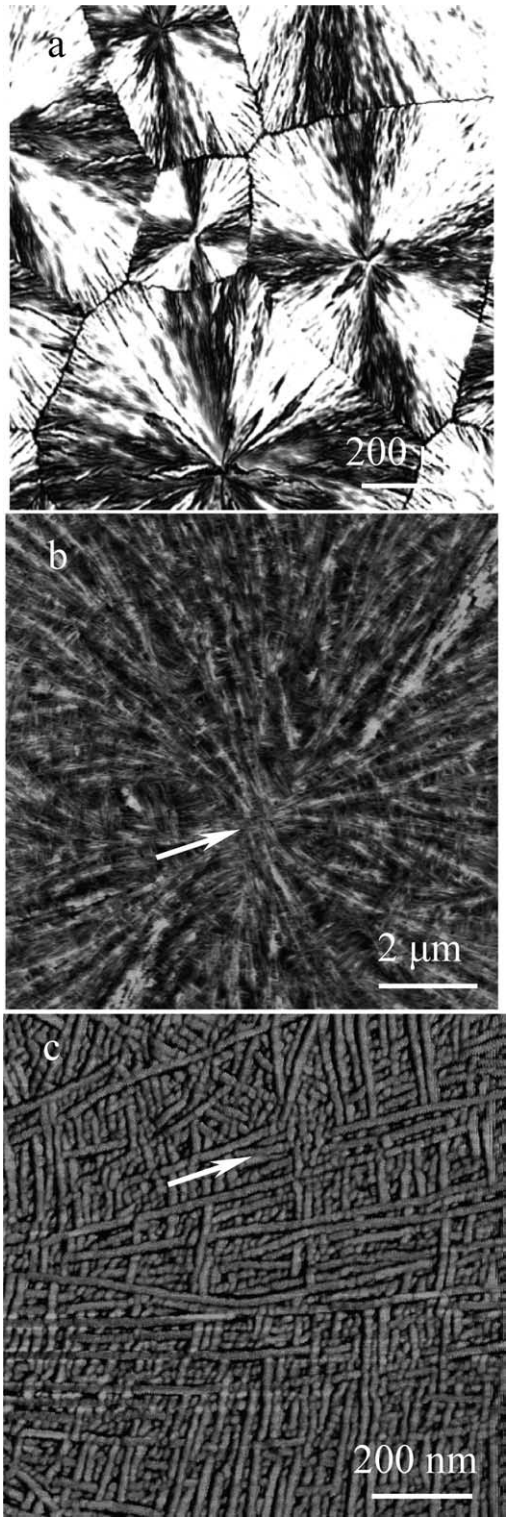

Fig. 1. *i*-PP type I spherulite crystallized at 130 °C for 6 h, (a) POM image, (b) AFM height image, and (c) phase image of lamellar structure. The radial direction was indicated by the arrow.

i-PP spherulites can be observed by AFM phase imaging, without the need of etching or staining, as shown in Fig. 1(c). Our results also indicate that the lamellar textures obtained by the AFM phase imaging are in agreement with those observed by TEM [7–10,24].

Type II spherulites with negative birefringence were obtained when the *i*-PP melts were crystallized at 145 °C, as

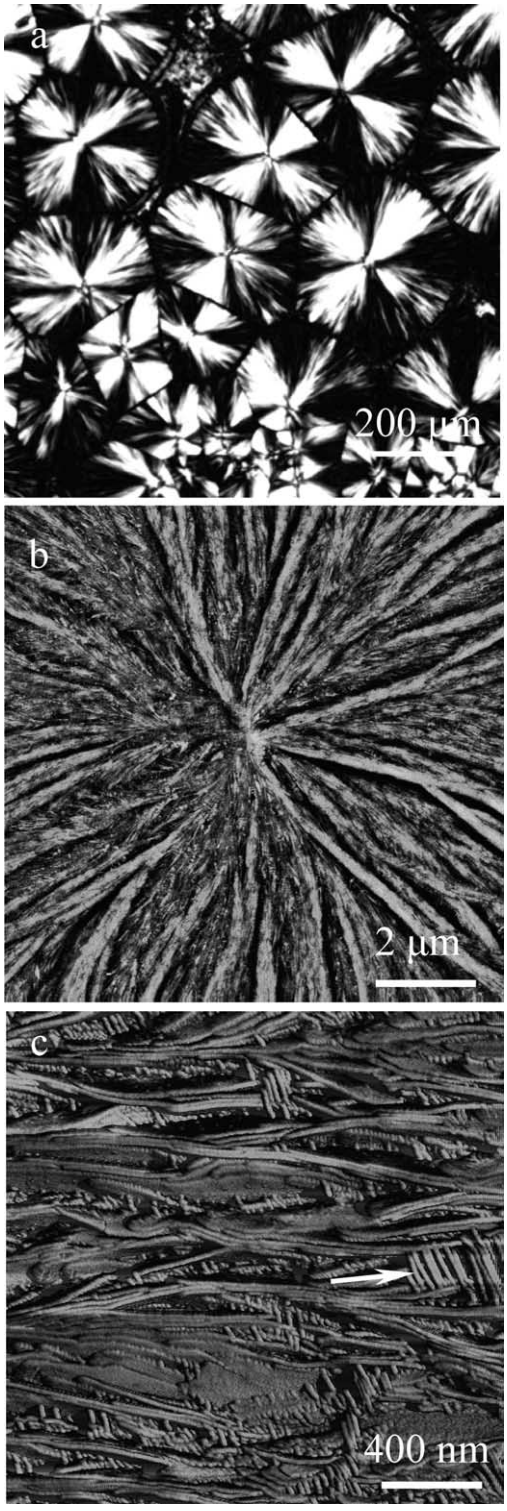

Fig. 2. *i*-PP type II spherulite crystallized at 145 °C for 6 h, (a) POM image, (b) AFM height image, and (c) phase image of the lamellar structure. The radial direction was indicated by the arrow in c.

shown in Fig. 2(a). The surface morphology of such spherulites was investigated by AFM height imaging, as shown in Fig. 2(b). A high resolution AFM phase image of the weakly cross-hatched lamellar structure of the spherulite is shown in Fig. 2(c). Here the lamellae are viewed edge-on. The difference between this image and that of Fig. 1(c) is that here the tangential lamellae are very short. It can be seen that the radial lamellae are dominant on the surface of the spherulite, and the normal negative birefringence of the spherulite is observed. The radial lamellae branch occasionally to form tangential lamellae, as indicated by the arrow in Fig. 2(c). The AFM phase image also clearly shows that the relative amount of the tangential lamellae is much less than for the type I spherulite, as seen in a comparison between Figs. 1(c) and 2(c).

Mixed type α-form spherulites are identified by random blue and yellow colors in the same quadrant when a color sensitive plate is inserted. Such spherulites are dominant over a wide range of crystallization temperatures. A POM micrograph of a mixed type spherulite without a clear Maltese cross, isothermally crystallized at 135 °C, is shown in Fig. 3(a). It is interesting to note that positive birefringence in the cores of the mixed type spherulites is usually observed, and that there the lamellar structures are similar to that of the type I spherulite, as indicated by arrows in Figs. 1(b) and 3(b). The dense cross-hatched lamellar textures in the mixed type spherulites core can be observed by AFM phase imaging. However, the lamellar textures surrounding the spherulitic cores consist of cross-hatched parent lamellae, seen face-on (the chain axis directed approximately normal to the image) and daughter lamellae. The face-on lamellae are commonly referred to as 'lath-like' lamellae, and we adopt that nomenclature thereafter. Fig. 3(c) is an AFM phase image of the interface between the cross-hatched and lath-like lamellae. In some regions of the mixed type spherulite, the small tangential crystals are so overgrown on the surface that we cannot see the underlying parent laths, as at the lower left of Fig. 3(c), while in other regions, the parent lamellae can be observed (upper right of Fig. 3(c)). The arrow in Fig. 3(c) indicates both the radial direction and the profusion of small tangential crystals overgrown on top of the underlying laths.

A β-form *i*-PP spherulite induced by a selective β-nucleating agent (the crystal of *N*,*N*′-dicyclohexyl-2,6-naphthalenedicarboxamide) at 130 °C is shown in Fig. 4(a). The selective β-nucleating agent is clearly seen and it can be observed that the β-form lamellae epitaxially crystallize on the lateral planes of the β-nucleating agent. Parallel edge-on β-form lamellae are clearly seen growing directly on one of the lateral surfaces of the crystal of the β-nucleating agent, as indicated by the arrow in Fig. 4(b), while in some areas away from the β-nucleating agent, flat-on lamellae with giant screw dislocations can be found, as shown in Fig. 4(c). Our results clearly show that the α- and β-form *i*-PP lamellae can be easily discriminated by AFM phase imaging.

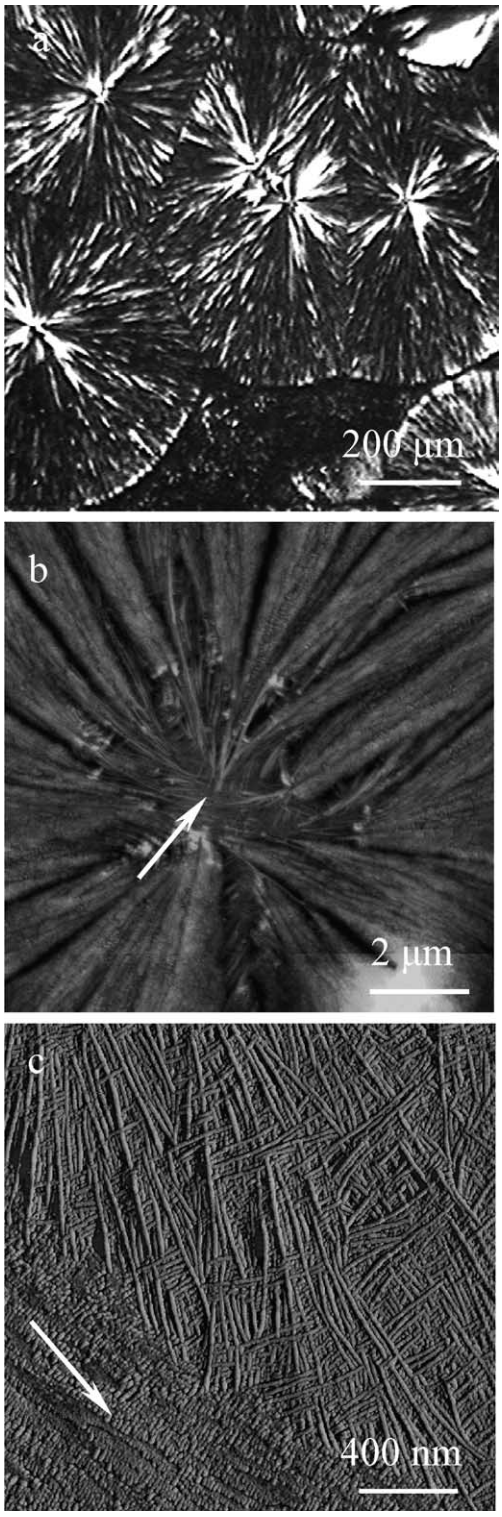

Fig. 3. *i*-PP mixed type α-form spherulite crystallized at 135 °C for 6 h, (a) POM image, (b) AFM height image, and (c) phase image of an interface between crosshatching and lath-like lamellae.

3.2. In situ dynamic observations: lamellar growth behaviors

The lamellar growth behaviors of α- and β-form *i*-PP

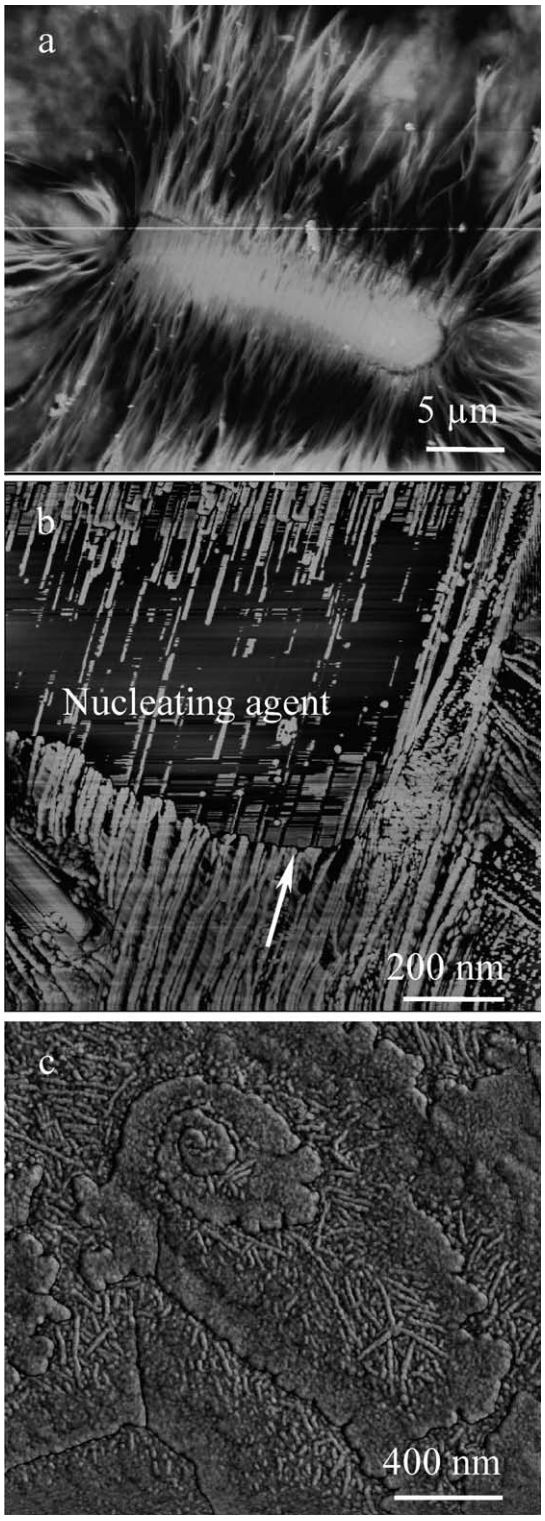

Fig. 4. *i*-PP type III β-form spherulite crystallized at 130 °C, (a) AFM height image, (b) AFM phase image of the interface between the nucleating agent and edge-on lamellae, and (c) AFM phase image of flat-on lamellae.

spherulites were studied with a high-temperature AFM in situ and in real time at various temperatures. The *i*-PP films were melted on the AFM hot stage at 200 °C and then crystallized at a selected temperature under N_2 protection. The crystallization temperatures of α-form *i*-PP spherulites were chosen between 140 and 162 °C in order to follow the lamellar growth using AFM. The crystallization rate of β-form *i*-PP lamellae from 140 to 152 °C is suitable for AFM observations in real time.

Consecutive high magnification phase images obtained in real time at 153 °C show the lamellar growth process in a type I α-form spherulite, as revealed in Fig. 5. Fig. 5(a) shows parent and daughter cross-hatched lamellae protruding into the melt. Radial parent lamellae protrude into the melt and the branches of tangential daughter lamellae develop, as indicated by the arrows in Fig. 5(b) and (c). The tangential lamellae branch from the parents behind the growing tips. The tangential lamellar branches may grow outward in only one direction, due to the restriction of space and the limitation of crystallizable melt, as indicated by the arrow in Fig. 5(d). The initial lamellar branching is shown at higher magnification in Fig. 6. The angle between the lamellar branches and the parent lamellae is observed to be approximately 80°, suggesting the formation of the α-modification through homoepitaxial growth on the (010) plane of a parent lamella, as indicated by arrows in Fig. 6(a) and (b). It has been proposed that α-form lamellar branching of *i*-PP is the result of the deposition of one layer of helices with the same chirality as the previous layer, with the helices of the new layer tilted 80° to the underlying helices in the (010) face of the parent lamella, resulting in the cross-hatched lamellar structures, as observed in Figs. 5 and 6. Occasionally, secondary branches can be observed. The secondary branches have an angle between branch and parent of about 40°, as indicated by the arrow in Fig. 6(c). In his study of the microstructure of α-form *i*-PP spherulites, Lovinger [10] found that various branching angles could be observed when thin films were examined, suggesting an effect of the mica substrate. However, the thickness of films in our observations was about 200 nm and crystallization was in the initial stage of the lamellar growth; so the small angle between the secondary branches and the parent lamellae might be an effect of the mica substrate or might be induced by other effects.

Recently, we have studied the edge-on lamellar branching of a poly(bisphenol A-codecane) polymer in real time at different crystallization temperatures [38]. It was found that lamellar branches occurred randomly on the parent lamellae at high degrees of supercooling. However, lamellar branches were seldom observed at crystallization temperatures near the melting point. The results shown now in Fig. 7 show that a similar result obtains for *i*-PP. Fig. 7 shows AFM phase images of the cross-hatched lamellar branching of *i*-PP developed at 146, 153 and 161 °C. Quantitative measurements show that the angle between the lamellar branches and the parent lamellae at all crystallization temperatures is approximately 80° and that at each temperature the lamellar branches and the parent lamellae have approximately the same growth rates. However, the lengths between the branch points and the tips of the parent

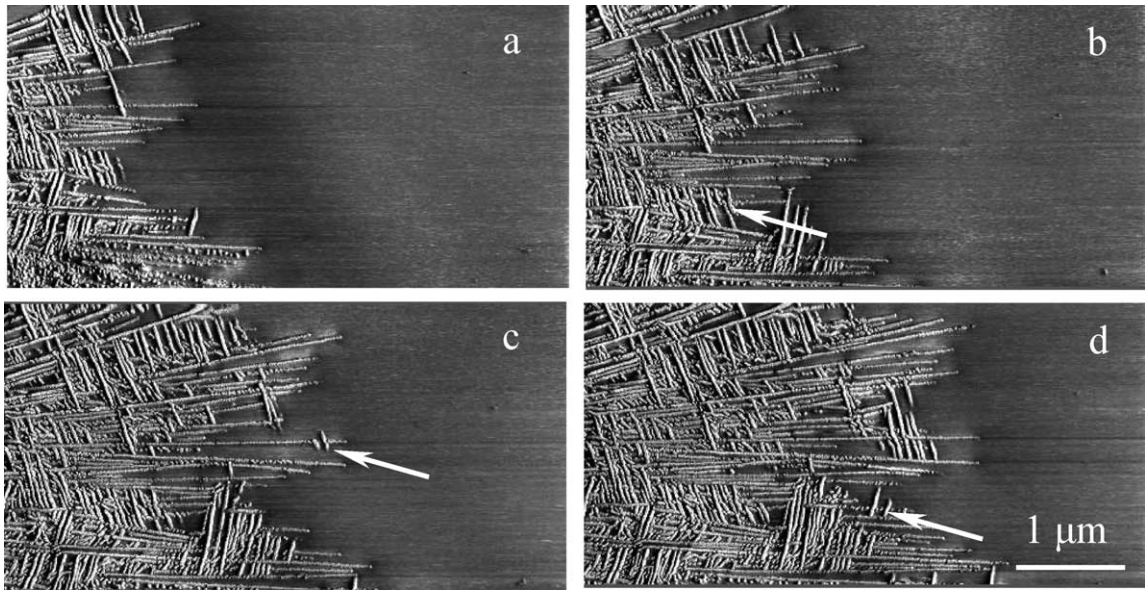

Fig. 5. The growth of cross-hatched lamellae crystallized at 153 °C and the time interval between two consecutive images is 3.6 min.

lamellae and the lengths between two branch points (the frequency branching) are significantly different at different crystallization temperatures. At about 146 °C, the branches were arranged fairly densely and regularly, as shown in Fig. 7(a) and (b). The consecutive AFM observations (Fig. 7(b)) were shifted to follow the growth front of the lamellae because the growth rate is too fast at 146 °C. The lengths between the branch points and the tips of the parent lamellae are approximately 100 nm, as shown in Fig. 7(a). At 153 °C, the frequency of lamellar branching is significantly lower than that of the lamellar branches crystallized at 146 °C, as shown in Fig. 7(c) and (d). In this case, the lengths between the branch points and the tips of the parent lamellae are in the range of 200–800 nm. At 161 °C (Fig. 7(e) and (f)), the frequency of lamellar branching is very small and the branches are very short. The radial lamellae are orderly and aligned almost parallel to each other. Some lamellae can grow above 1 μm without any branches. A comparison of the phase images of the lamellar branching in Fig. 7 indicates that the thickness of the lamellae grown at 153 and 161 °C appear to be larger than that of the lamellae developed at 146 °C. The average widths of the lamellae at high temperatures could not be accurately measured because of the broadening effects caused by different AFM tips and different set-point amplitude ratios. However, it can be seen that the parent and branching lamellae formed at the same crystallization temperature show no significant difference in average width.

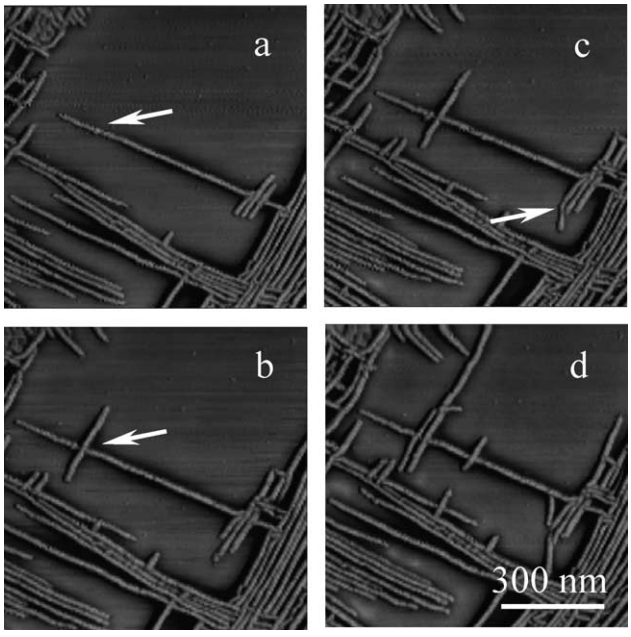

Fig. 6. The branching behavior of the cross-hatched lamellae crystallized at 153 °C and the time interval between two consecutive images is 5.3 min.

Fig. 8 is an AFM phase image showing the growth of lath-like α-form *i*-PP lamellae at 156 °C in real time. The lath-like lamellae are stacked, and a second or a third layer can be found growing on top of the first lath-like lamellar layer, as indicated by arrows in Fig. 8(b). As the lath-like lamellae grow forward, many small crystals form at both sides of a lath at the same temperature, as indicated by arrows in Fig. 8(c). The small crystals are believed to be the initial stage of the lamellar branching through the homo-epitaxial growth on the (010) plane of a lath-like parent lamella. It is impossible to determine the branching angle between the lamellar branches and the parent lath using AFM because the lengths (*b* axis) of the lamellar branches are too short. The growth rate of the lamellar branches in the *b* direction cannot be obtained, due to the short observation time.

Fig. 9 shows AFM phase images of lath-like lamellae

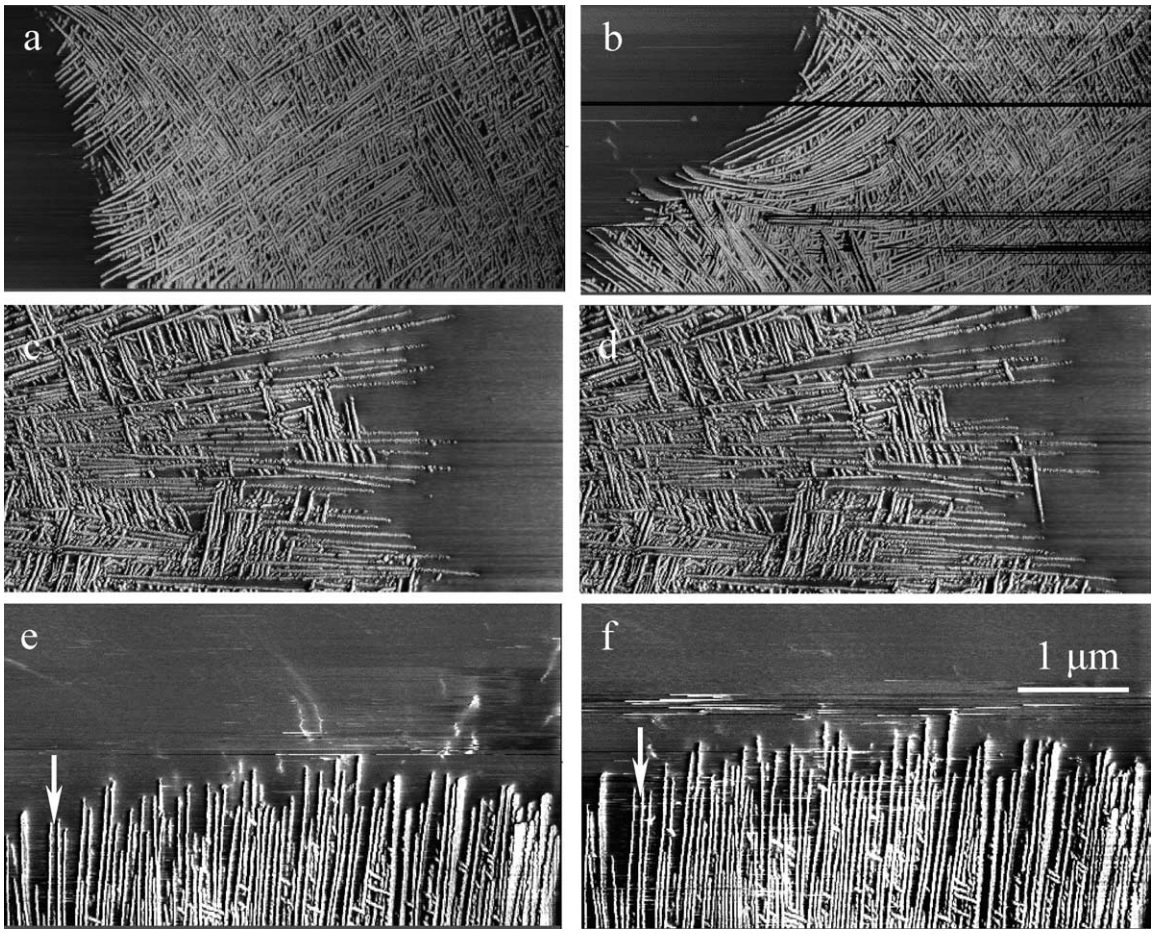

Fig. 7. The branching of the cross-hatched lamellae at different temperatures, (a) and (b) 146 °C; (c) and (d) 153 °C; (e) and (f) 161 °C.

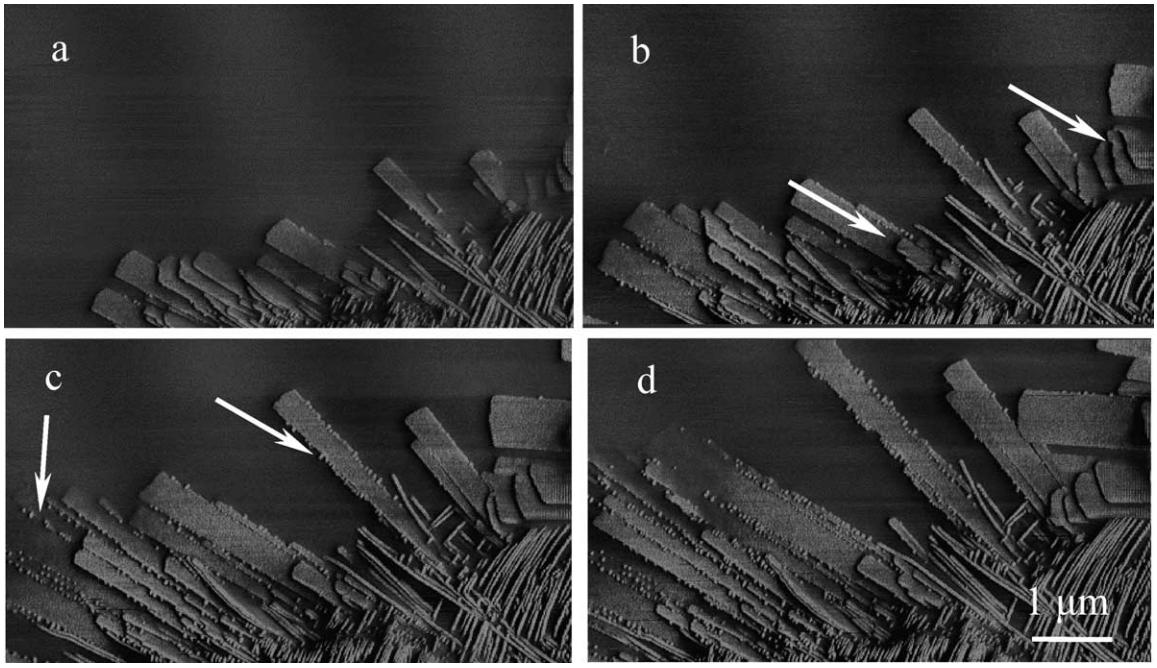

Fig. 8. The growth of lath-like lamellae crystallized at 156 °C and the time interval between two consecutive images is 3.6 min.

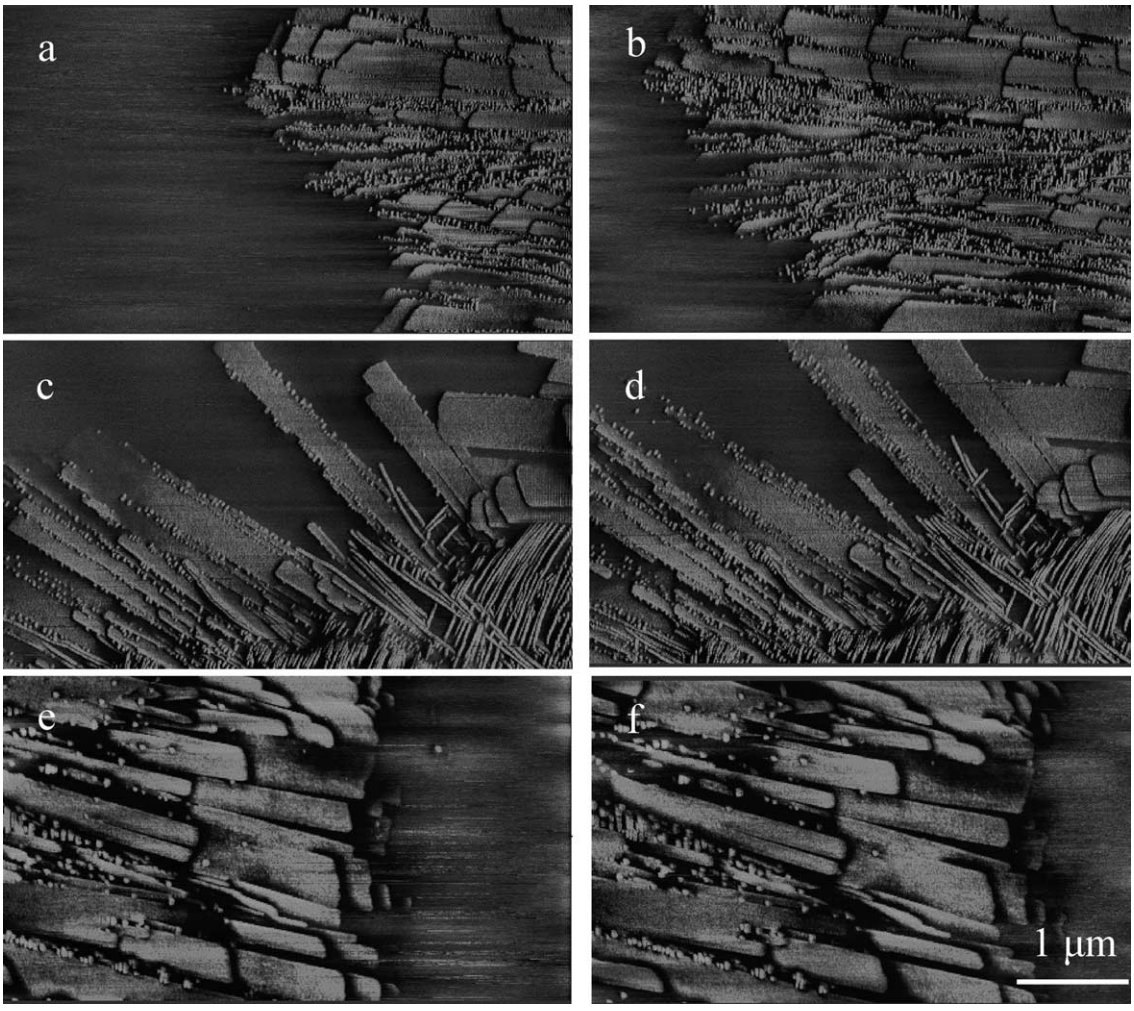

Fig. 9. The branching of the lath-like lamellae at different temperatures, (a) and (b) 145 °C; (c) and (d) 154 °C; (e) and (f) 160 °C.

developed at 145, 154 and 160 °C. It is seen that the frequency of the initial lamellar branches on the (010) planes of the lath-like lamellae developed at high degrees of supercooling is much larger than that for crystallization temperatures nearer the melting point. At about 145 °C, the density of the initial lamellar branches on the (010) plane is fairly high, as shown in Fig. 9(a) and (b). Some branches can occur at the growing tips of the lath-like parent lamellae, as shown in Fig. 9(b). At 154 °C, the frequency of lamellar branching is significantly lower than that of the lamellar branches crystallized at 145 °C, as shown in Fig. 9(c) and (d). In this case, the lamellar branches seldom appear at the growing tips of the parent lamellae, as seen in Fig. 9(c). At 160 °C (Fig. 9(e) and (f)), the frequency of lamellar branching is very small. This is a continuation of the trend observed in the branching of edge-on lamellae seen at lower crystallization temperatures (c.f., Fig. 7).

Different from the lamellar growth of α-form *i*-PP spherulites, β-form spherulites usually exhibit broad lamellae with the chain axis approximately normal to the substrate and containing numerous giant screw dislocations [23]. Fig. 10 shows growth parallel and normal to the substrate at 147 °C using AFM in real time. As the flat-on lamellae grow forward, the growth fronts expanded outward in all directions. The radial growth direction cannot be discriminated from the small area scanned by AFM due to the expanding growth mode. The spiral growth at a screw dislocation can be seen in Fig. 10(b) and (c). The hexagonal profile of the β-form flat-on lamellae with at least three sides develops during the observations, as shown in Fig. 10(c) and (d).

From our real time AFM observations, it is found that the α- and β-form lamellae can be easily distinguished by AFM, since the lamellar shape, the branching and the growth behaviors are significantly different. Moreover, the growth of the flat-on lamellae of β-form *i*-PP without the formation of any lamellar branches suggests that the trigonal lattice of the β-form *i*-PP crystals is not suitable for homoepitaxial growth.

3.3. Growth kinetics

The average growth rates of α- and β-form lamellae were determined by measuring the length of a specific lamella in

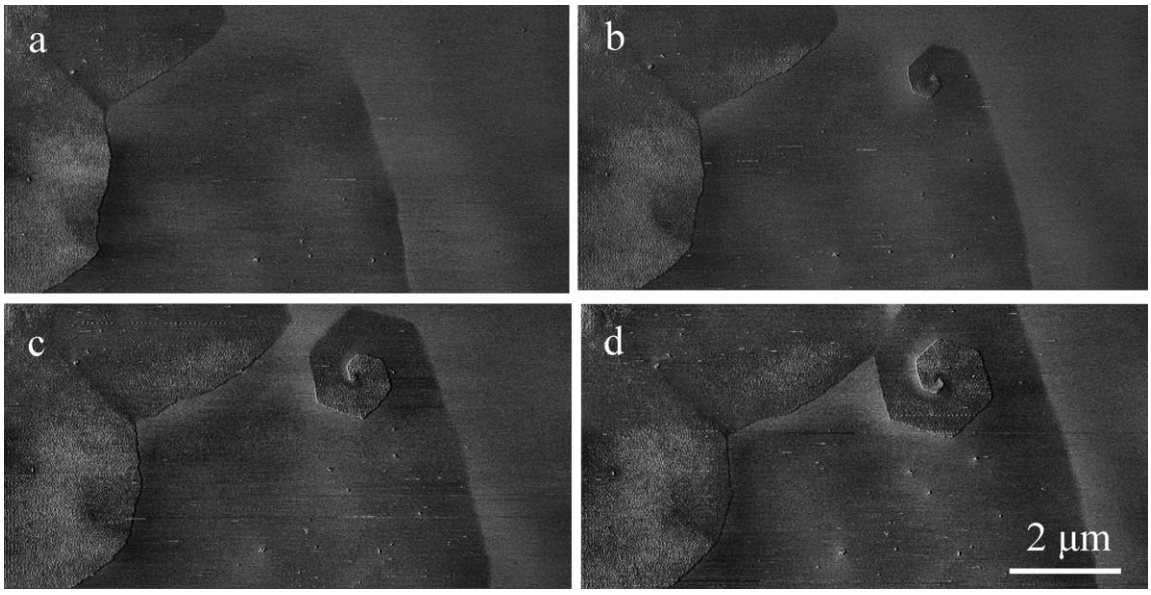

Fig. 10. The growth of flat-on β-form lamellae at 147 °C and the time interval between two consecutive images is 5.3 min.

consecutive time intervals using AFM at different temperatures. At the growing front of a spherulite, the average growth rate is identically constant for either a cross-hatched (edge-on) or a lath-like (face-on) α-form lamella (as expected), as shown in Fig. 11(a). However, for the second or third layer of lath-like α-form lamellae, the average growth rate became very slow, due to the lack of sufficient crystallizable material (c.f. Fig. 9) [39–41]. The average growth rates (averaged over several lamellae of both edge-on and flat-on orientations) of α- and β-form lamellae at different temperatures are shown in Fig. 11(b). The cross-hatched and lath-like α-form lamellae had nearly the same growth rate at the same crystallization temperature and only the average growth rate of lath-like lamellae is presented in Fig. 11(b). The average α-form lamellar growth rate increased significantly with decreasing crystallization temperature, from 65 nm min^{-1} at 162 °C to 750 nm min^{-1} at 140 °C. The average growth rate of flat on β-form lamellae also increased with decreasing crystallization temperature, from 120 nm min^{-1} at 152 °C to 840 nm min^{-1} at 140 °C. The average lamellar growth rate of β-form lamellae was much lower than that of α-form lamellae when crystallization temperature increased from 147 to 152 °C. This is at least partially due to the lower equilibrium melting temperature of the β-form relative to the α-form crystals, leading to a lower degree of supercooling for the β-form. However, the discrepancy of growth rates diminishes with decreasing temperature and essentially vanishes at 140 °C.

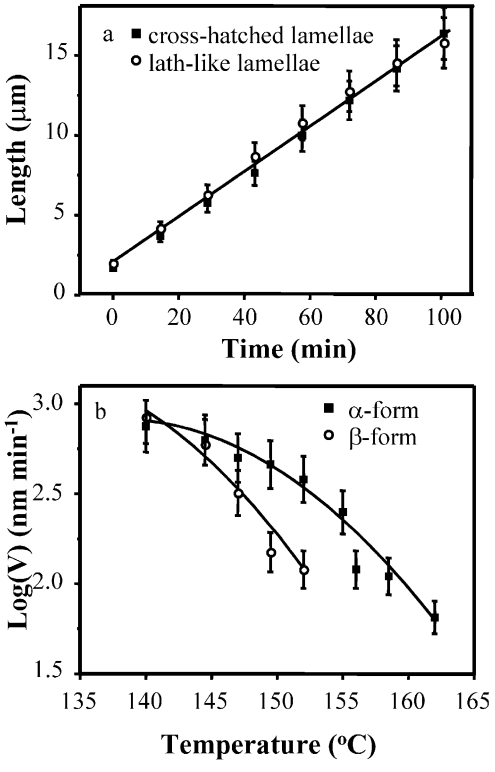

Fig. 11. The lamellar growth rates determined by AFM: (a) the growth rates of crosshatched and lath-like lamellae at 156 °C and (b) the lamellar growth rates at different crystallization temperatures.

It is known that the growth of a lamella involves the diffusion of uncrystallizable or poorly crystallizable chains from the growth front, resulting in the buildup of such materials in the melt adjacent to the growth front. The steady state growth of the crystals is dictated by the adjustment of the growth rate to the rate at which the uncrystallizable material can diffuse away. In thin films, the buildup of such 'impurities' near the growth front is manifested in a local increase in film thickness [41]. At the same time, the density difference between crystal and melt produces both a decrease in the height of the crystallized material, relative to the melt, and a trough in

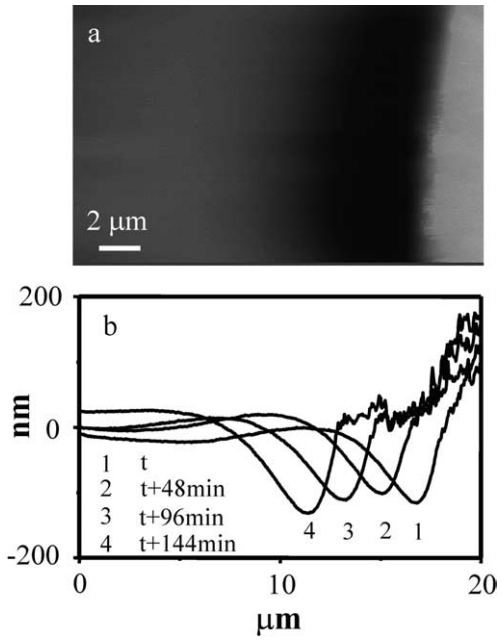

Fig. 12. AFM height image and the height profiles to show the depletion of molten lathlike lamellae (a) AFM height image; (b) the height profiles at different crystallization time.

the melt near the growth front [41]. The formation of such a depletion trough is dictated by the inability of new molten polymer to diffuse to the growth front as rapidly as the density difference depletes polymer at the front. Fig. 12(a) shows an AFM height image. The corresponding height profiles (Fig. 12(b)) show the large depletion trough of the molten polymer at 162 °C in the melt near the growing front of lath-like α-form lamellae and also the smaller increase in film thickness due to impurity buildup in the melt immediately adjacent to the growth front. These results agree qualitatively with the conceptual model just described, but diffusivities computed from measured growth velocities and diffusion lengths are some two orders of magnitude greater than diffusivities measured in bulk polyethylene.

4. Conclusions

POM and AFM images of types I, II and mixed α-form spherulites are compatible, with amounts of radial and tangential lamellae. β-form structures, on the other hand, exhibit very broad crystal lamellae, with very visible giant screw dislocation growth spirals. It is shown that the several spherulite types are easily differentiable by AFM.

In situ observations of crystallization demonstrate that the frequency of tangential branching from radial α-form lamellae increases with decreasing crystallization temperature. At any given temperature, flat-on and edge-on lamellae grow at the same rate. Where measurable, leading radial lamellae and transverse branches grow at the same rate, while trailing lamellae grow at a slower rate. Height profiles during growth exhibit a small increase of height of the melt directly adjacent to the interface, followed by a trough, evidence of exclusion of molecules by the growing crystals and an inability of the melt to rapidly replenish the melt near the interface.

Acknowledgements

We are grateful for the support of the Outstanding Youth Fund and the National Science Foundation of China and the Hong Kong Government Research Grants Council Joint Research Scheme under Grants No. N_HKUST 618/01. This work is also supported by the MOST (No. 2003CB615600) and CAS program (No. KJCX2-SW-H07).

References

[1] Padden FJ, Keith HD. J Appl Phys 1959;30:1479–84.
[2] Keith HD, Padden FJ, Walter NM, Wyckoff HW. J Appl Phys 1959; 30:1485–8.
[3] Turner-Jones A, Aizlewood JM, Beckett R. Makromol Chem 1964; 75:134–46.
[4] Marrow DR. J Macromol Sci Phys 1969;B3:53–65.
[5] Brückner S, Meille SV, Petraccone V, Pirozzi B. Prog Polym Sci 1991;16:361–404.
[6] Androsch R, Wunderlich B. Macromolecules 2001;34:5950–60.
[7] Norton DR, Keller A. Polymer 1985;26:704–16.
[8] Padden FJ, Keith HD. J Appl Phys 1966;37:4013–20.
[9] Binsbergen FL, De Lange BGM. Polymer 1968;9:23–40.
[10] Lovinger AJ. J Polym Sci, Polym Phys Ed 1983;21:97–110.
[11] Lotz B, Wittmann JC. J Polym Sci, Polym Phys Ed 1986;24:1541–58.
[12] Lotz B, Wittmann JC, Lovinger AJ. Polymer 1996;37:4979–92.
[13] Crissman JM. J Polym Sci 1969;A2:389–404.
[14] Fujiwara Y. Colloid Polym Sci 1975;253:273–82.
[15] Lovinger AJ, Chua JD, Gryte LC. J Polym Sci, Polym Phys Ed 1977; 15:641–57.
[16] Li HH, Zhang X, Kuang X, Wang JJ, Wang D, Li L, et al. Macromolecules 2004;37:2847–53.
[17] Vancso GJ, Liu G, KargerKocsis J, Varga J. Colloid Polym Sci 1997; 275:181–6.
[18] Turner-Jones A, Cobbold AJ. J Polym Sci 1968;6:539–46.
[19] Leugering H. J Makromol Chem 1967;109:204–16.
[20] Varga J. J Mater Sci 1992;27:2557–79.
[21] Varga J. J Macromol Sci Phys 2002;B41:1121–71.
[22] Matheu C, Thierry JC, Wittmann JC, Lotz B. J Polym Sci, Polym Phys Ed 2002;40:2504–15.
[23] Haeringen DTV, Varga J, Ehrenstein GW, Vancso GJ. J Polym Sci, Polym Phys Ed 2000;38:672–81.
[24] Bassett DC, Olley RH. Polymer 1984;25:935–43.
[25] Li JX, Cheung WL, Chan CM. Polymer 1999;40:3641–56.
[26] Nishida K, Konishi T, Kanaya T, Kaji K. Polymer 2004;45:1433–7.
[27] Stocker W, Schumacher M, Graff S, Thierry A, Wittmann JC, Lotz B. Macromolecules 1998;31:807–14.
[28] Kikkawa Y, Abe H, Iwata T, Inoue Y, Doi Y. Biomacromolecules 2001;2:940–5.
[29] Pear R, Vancso GJ. Macromolecules 1997;30:5843–8.
[30] Schultz JM, Miles MJ. J Polym Sci, Polym Phys Ed 1998;36:2311–25.
[31] Ivanov DA, Amalou Z, Magonov SN. Macromolecules 2001;34: 8944–52.
[32] Godovsky YK, Magonov SN. Langmuir 2000;16:3549–52.

[33] Hobbs JK, Humphries ADL, Miles MJ. Macromolecules 2001;34: 5508–19.
[34] Hobbs JK, Miles MJ. Macromolecules 2001;34:353–5.
[35] Schőnherr H, Wilyatno W, Pople J, Frank CW, Fuller GG, Gast AP, et al. Macromolecules 2002;35:2654–66.
[36] Schőnherr H, Waymouth RM, Frank CW. Macromolecules 2003;36: 2412–8.
[37] Schőnherr H, Bailey LE, Frank CW. Langmuir 2002;18:490–8.
[38] Jiang Y, Yan DD, Gao X, Han CC, Jin XG, Li L, et al. Macromolecules 2003;36:3652–5.
[39] Kit KM, Schultz JM. J Polym Sci, Polym Phys Ed 1998;36:873–88.
[40] Xu J, Guo BH, Zhang ZM, Zhou JJ, Jiang Y, Yan SK, et al. Macromolecules 2004;37:4118–23.
[41] Duan YX, Jiang Y, Jiang SD, Li L, Yan SK, Schultz JM. Macromolecules 2004;37:9283–6.